Research in Pharmaceutical Sciences, October 2025; 20(5): 701-711
Received: 14-04-2024
Peer Reviewed: 07-07-2024
Revised: 08-10-2024
Accepted: 12-10-2024
Published: 20-10-2025

School of Pharmacy & Pharmaceutical Sciences
Isfahan University of Medical Sciences

Original Article

Synthesis of carbon quantum dots from garlic juice and evaluation of their cytotoxic and apoptogenic effects on cancer cells

Fereshteh Jalilian[1], Ali Barati[2], Ehsan Yousefi[3], Leila Hosseinzadeh[1,*], and Elham Arkan[4,*]

[1]*Pharmaceutical Sciences Research Center, Health Institute, Kermanshah University of Medical Sciences, Kermanshah, Iran.*
[2]*Faculty of Chemistry, Razi University, Kermanshah, Iran.*
[3]*Student Research Committee, Kermanshah University of Medical Sciences, Kermanshah, Iran.*
[4]*Nano Drug Delivery Research Center, Kermanshah University of Medical Sciences, Kermanshah, Iran.*

Abstract

Background and purpose: Carbon quantum dots (CQDs) have garnered significant interest in various fields as a burgeoning category of photoluminescent nanomaterials. The current study involved the synthesis of photoluminescent carbon dots through the hydrothermal processing of garlic (Allium sativum L.) juice, serving as a naturally derived carbon source.
Experimental approach: The morphology and optical properties of the carbon dots were characterized by TEM, XRD, FT-IR, XPS, UV-Vis, and photoluminescence. The cytotoxic and apoptotic effects of CQDs were evaluated in A549, SKNMC, and H1299 (p53 null) human carcinoma cell lines.
Findings/Results: The TEM findings confirmed that carbon dots exhibit a limited variability in their size distribution, characterized by mean diameters of around 16.3 ± 2.7 nm. The peak emission wavelength of carbon dots was observed at 400 nm, accompanied by an excitation peak at 320 nm, and their quantum yield in aqueous solution was measured to be 11.5%. The garlic CQDs were proven to be extremely potent cytotoxic agents, especially against H1299 cells. Apoptosis induction by CQDs was accompanied by an increase in activation of caspase-3 and caspase-9, as well as the disruption of mitochondrial membrane potential in H1299 cells.
Conclusion and implications: The apoptotic potential of garlic CQDs was evaluated in the most sensitive cell line, H1299. The apoptogenic effect of garlic CQDs on H1299 cells is important because it has been demonstrated that the loss of p53 is associated with poor clinical prognosis in cancer treatment.

Keywords: Apoptogenic activity; Carbon quantum dot; Garlic; Photoluminescence.

INTRODUCTION

Today, a variety of photoluminescent nanomaterials (1), such as biocompatible gold and silver nanodots or nanoclusters (2,3), rare-earth doped up-conversion nanoparticles (4), and semiconductor quantum dots (5,6), are widely employed in different medical fields like the detection and diagnosis of disease, bioimaging, drug delivery, and even therapy (7). However, the low quantum yield, poor photostability, and expensive precursors significantly limit the application of these nanomaterials. More importantly, the toxicity of these nanomaterials has always been a serious cause for concern (3,8).

Carbon quantum dots (CQDs) are considered a novel addition to the category of photoluminescent nanomaterials and have garnered significant interest across a wide variety of disciplines. They were first observed during the purification of single-walled carbon nanotubes derived from the arc-discharge of soot in 2004 (9,10). CQDs exhibit exceptional characteristics such as advantageous water solubility, compatibility with biological systems, a high quantum yield (11,12), bio-imaging and biomolecule/drug delivery (6), and catalysis (13).

*Corresponding authors:
L. Hosseinzadeh, Tel: +98-8334266780, Fax: +98-8334276493
Email: lhoseinzadeh@kums.ac.ir
E. Arkan, +98-8334266780, Fax: +98-8334276493
Email: Elhamarkan@kums.ac.ir

Access this article online	
	Website: http://rps.mui.ac.ir
	DOI: 10.4103/RPS.RPS_28_24

Furthermore, the presence of carboxylic and alcoholic functional groups on the CQDs' surface enables straightforward manipulation of these nanomaterials through the attachment of diverse functional groups or their bonding with multiple therapeutic agents intended for biological uses (14). Numerous reports support the fact that CQDs present lower cytotoxicity compared to other photoluminescent nanoparticles, especially those comprising toxic heavy metal ions, and provide an ideal alternative for *in vivo* applications.

Various methods, including laser ablation (15), electrochemical (10) and chemical carbonization (16), hydrothermal carbonization (17) or microwave irradiation (18) have been developed to synthesize CQDs from different starting materials. Among them, the hydrothermal method can be taken into account as a proper approach for the synthesis of CQDs from different sources (19).

Despite the variety of chemical carbon sources, recently a great deal of attention has been devoted to using natural and biological materials like biomass, different fruit juices (20), and waste materials (21) as an initial source to synthesize CQDs. These materials usually contain different ingredients that can be easily converted into CQDs under hydrothermal conditions (22). Interestingly, reports suggest that the initial CQD precursor plays an important role in determining the optical properties and biological activities of CDs. For example, Hsu *et al*. prepared photoluminescent CQDs from green tea that possessed high inhibition efficiency for human breast cancer cells (MDA-MB-231) without damage to normal cells (23). They also reported CQDs prepared from ginger that exhibited extremely high suppression efficiency on the growth of human hepatocellular carcinoma cells (HepG2), with low toxicity for normal mammary epithelial cells (MCF-10A) and mouse liver cells (FL83B). The inhibition efficiency of these CQDs on HepG2 cells was selective over other cancer cells, such as human lung cancer cells (A549), human breast cancer cells (MDA-MB-231), and human cervical cancer cells (HeLa). These interesting observed properties were attributed to the intrinsic antioxidative, anti-carcinogenic, and anti-inflammatory properties of the components found in green tea and ginger. In this regard, it is well known that the active compounds in garlic have anticancer properties (24). In a study conducted by Sun *et al*. CQDs synthesized by garlic, in comparison to other natural materials, exhibited a high content of nitrogen and sulfur elements (25). Throughout ancient history, garlic has been widely used due to its health and medicinal properties for the treatment of diseases such as heart disease and infections, and as an agent in cancer prevention (15). Findings demonstrate that garlic has a significant impact in inhibiting the growth and development of cancer cells in different tissues, such as hepatoma, mammary, squamous cell carcinoma of the skin, esophagus, and colon cancer (26). This beneficial outcome has stimulated further studies of the anticancer properties of garlic.

In the present study, we employed the hydrothermal method to prepare CQDs from garlic juice to evaluate their cytotoxic effects on different cancer cells. The presence of many amino and carboxyl groups on the surface of the prepared CQDs resulted in their high water solubility and high stability in high-ionic-strength media. The cytotoxic effect of CQDs was evaluated on H1299 (human non-small cell lung carcinoma), SKNMC (human neuroblastoma), and A549 (human lung carcinoma) cell lines. Given the importance of apoptotic cell death as a key feature of a potential chemotherapeutic drug, the apoptotic potential of the CQDs was evaluated on the most sensitive cell line, H1299, in the next experiments.

MATERIALS AND METHODS

Materials

All reagents of analytical grade were utilized in their received form, with the assurance of utmost purity being the governing criterion for selection. Hydrazine and ammonium bromide were purchased from Merck (Germany). Phosphate-buffered solution (PBS, 0.1 M) at pH 7.4 was used. Garlics were obtained from Toyserkan, Iran. 3-(4,5-Dimethylthiazol-2-yl)-2,5-diphenyltetrazoliumbromide (MTT), rhodamine caspase 9 substrate, and caspase-3

detection kit were bought from Sigma Aldrich (St. Louis, MO, USA). Cell culture medium, penicillin, streptomycin, and fetal bovine serum (FBS) were purchased from Gibco (Gibco, Grand Island, NY, USA).

Apparatus

Spectrophotometric measurements were conducted utilizing a Varian Cary Eclipse spectrofluorometer, which was furnished with a xenon flash lamp. Transmission electron microscopy (TEM) images were acquired using a Zeiss-EM10C transmission electron microscope operating at an accelerating voltage of 80 kV. To study the chemical structures of CQDs, Fourier transform infrared spectroscopy (FTIR) manufactured by Shimadzu Company (Japan) was used. X-ray diffraction (XRD; SEIFERT, PTS3003, Germany) was used to identify the structure of the CQDs.

Fluorescence microscopy images were obtained from a fluorescent microscope (Olympus IX71; Japan) with blue light as the excitation source.

Synthesis of CQDs

The one-step hydrothermal treatment was used to prepare CQDs from garlic juice as a bio-derived precursor.

In the present study, the CQDs were prepared as follows. The cloves of garlic were minced (200 g) with a food processor and then pressed to extract crude garlic juice. To remove large particles and obtain a clear juice, the raw juice underwent filtration using filter paper with a low filtration rate, followed by centrifugation of the resulting liquid for 30 min at 6000 rpm three times. Afterward, 10 mL of the garlic juice was diluted to 40 mL of distilled water and transferred into a 100 mL Teflon-lined stainless steel laboratory autoclave and heated in an oven at a constant temperature of 180 °C for 7 h. The black carbonized solution was cooled to room temperature. The solution was centrifuged at 3000 rpm for 30 min to remove large or agglomerated particles. The supernatant containing CQDs was filtered through a 0.2 µm membrane to remove large particles. Then, the brownish supernatant was dialyzed against ultrapure water through a dialysis membrane (MWCO¼ 3.5-5 kD, Float-A-Lyzer G2, Spectrum Laboratories, Rancho Dominguez, CA, USA) for 3 days. The solution containing CQDs was dried at 50 ℃ for 24 h.

While a definitive and intricate process for the synthesis of CQDs from such materials remains elusive, a plausible mechanism can be proposed, drawing from existing literature, particularly regarding the carbonization of carbohydrates. This proposed mechanism likely involves several key stages, such as dehydration, polymerization, carbonization, aromatization, and nucleation.

In addition, the growth mechanism of the carbonaceous materials in the hydrothermal method can be well described using the LaMer model (27). According to the LaMer model, when the concentration of aromatic clusters in the aqueous solution reaches a critical amount, the nucleation process takes place. This process finally results in a core-shell structure with a hydrophobic core and a hydrophilic shell that is less dehydrated and contains a large number of reactive oxygen functional groups.

Quantum yield measurements

Experimentally, the relative fluorescence quantum yield of prepared CQDs was determined at an excitation wavelength of 320 nm using the following equation:

$$Q_x = Q_r \left(\frac{I_x}{I_r}\right)\left(\frac{A_r}{A_x}\right)\left(\frac{\eta_x^2}{\eta_r^2}\right)$$

Where r and x refer to the standard reference and the sample of interest, respectively, Q is the quantum yield, I is the integrated emission spectra, η is the refractive index of the solvent, and A is the absorbance. To avoid self-absorption effects, the absorbance was kept below 0.1 quinine sulfate in 0.1 M H2SO4, using the already known quantum yield of 0.54 as a standard reference.

Cell culture

The H1299 cell line was a kind gift from Prof. G. Storm. The cells have a homozygous partial deletion of the p53 protein and lack p53 protein expression. SKNMC and A549 were obtained from the Pasteur Institute (Tehran, Iran). SKMNC represents a neuroepithelioma cellular lineage that originated from a metastatic supraorbital neoplasm in the human

brain (28). A549 cells are human adenocarcinoma basal epithelial cells (10). The cells were cultured in Dulbecco's modified Eagle's medium (DMEM-F12) with 5% (v/v) FBS, 100 U/mL penicillin, and 100 mg/mL streptomycin. The medium was changed 2-3 days after and was sub-cultured when the cell population density reached 70-80% confluence.

Assay of inhibitory effects of CQDs on the growth of human carcinoma cell lines

The *in vitro* inhibitory effects of garlic CQDs on the growth of H1299, A549, and SKNMC cells, and also HUVEC as a model of normal cells, were evaluated by MTT assay. Briefly, the cells were suspended in DMEM supplemented with 10% bovine serum, 100 units/mL of penicillin, and 100 µg/mL of streptomycin at a concentration of 1×10^5 cells/mL. The cell suspension was pipetted into a 96-well plate (100 µL /well) and was permitted to adhere in a humidified incubator containing 5% CO_2 at 37 °C. One day after seeding, the cells were treated with fresh medium with different concentrations (0-100 µg/mL) of CQDs dissolved in culture medium and incubated for 48 h. The medium was removed and replaced by 100 µL of 0.5 mg/mL of MTT in growth medium, and then the plates were transferred to a 37 ℃ incubator for 3-4 h. Next, the supernatants were removed carefully, and 100 µL of dimethyl sulfoxide was added to each well for the dissolution of formazan crystals. Then, the absorbance of each well at 570 nm was determined using an ELISA plate reader (Synergy-2, BioTek Instruments Inc., Winooski, VT, USA). The IC_{50} value was calculated by plotting the $\log_{10}$ of the percentage of proliferation versus concentration. Furthermore, cell images were captured 24 h post-treatment at a 20x magnification utilizing a Matic microscope outfitted with a Leica digital camera.

Cellular uptake

For evaluation of CQD uptake, cells were cultured on a 12-well cell culture plate for 24 h to achieve approximately 80% confluence. A concentrated aqueous CQD solution (0-20 µg/mL) was added to designated wells. After incubation for 6 h, the culture medium containing garlic CQDs was discarded. Then, cells were lysed with 1% Triton X-100. The fluorescence was measured at an excitation wavelength of 340 nm and an emission wavelength of 450 nm using a fluorescence microplate reader (BioTek, H1M, USA). For fluorescence microscopy images, cells were plated onto 12-well plates at a density of 5.0×10^5 cells/well and in a volume of 1 mL. The cell culture medium was then replaced with fresh medium containing the garlic CQDs in a concentration of 20 µg/mL and incubated for 6 h at 37 °C in a 5% CO_2/95% air atmosphere. Fluorescence images were taken at a magnification of 100x under a fluorescence microscope (Model: Micros Austria) with an imaging system. Cells without any paraquat treatment were taken as a staining control.

Assessment of mitochondrial membrane potential

Mitochondria have been shown to play a key role in the induction of apoptosis. In the current study, rhodamine 123 fluorescent dye, a cell-permeable cationic dye, was used for monitoring mitochondrial membrane potential (MMP). Depolarization of MMP during cell apoptosis results in the loss of rhodamine 123 from the mitochondria and a decrease in intracellular fluorescence intensity (29). At the end of treatment, cells were incubated with rhodamine 123 for 30 min at 37 °C. The fluorescence intensity was measured at an excitation wavelength of 488 nm and an emission wavelength of 520 nm using a fluorescence microplate reader (BioTek, H1M, USA).

Measurement of caspase-3 and 9 activities

The activity of caspase-3 was assessed under the guidelines outlined in the manual provided by the Sigma/Caspase-3 assay kit. Briefly, H1299 cells were detached and lysed with lysis buffer with appropriate protease inhibitors. The cell lysate was centrifuged for 10 min at 14000 rpm. Next, the supernatant was transferred to a tube and mixed with caspase-3 and caspase-9 substrates. After 1 h incubation at 37 °C, the absorbance of the chromophore p-nitroanilide was detected by a microplate reader at 405 nm. H1299 cells were cultured in

the absence of CQD to serve as the control group, and the results were quantified as a percentage relative to the control.

Statistical analysis

Data were evaluated with GraphPad Prism 5.0 software, and the results have been provided as mean ± SEM. The data were compared using the one-way analysis of variance (ANOVA), followed by the Tukey test. A *P*-value of less than 0.05 was considered statistically significant.

RESULTS

Characterization of CQDs

The obtained results indicated the formation of such structures from garlic during the hydrothermal process. FTIR spectra were employed to analyze the surface functional groups present on the CQDs (Fig. 1A). The broad band at 3200-3550 cm^{-1} was assigned to C-OH and N-H stretching vibrations, and the peak at 2800-2950 cm^{-1} was attributed to the C-H stretching vibrations. The bending vibrations of the N-H could appear at 1400 $cm^{-1,}$ and peaks at about 1600 and 1280 cm^{-1} indicated the presence of C=O and C-NH-C stretching vibration, respectively. The band at around 1066 cm^{-1} presented the existence of C-O (hydroxyl, ester, epoxide, or ether) groups. The presence of these functional groups on the surface of CQDs led to their exceptional aqueous solubility without requiring additional chemical alterations.

The XRD pattern of the synthesized CQDs (Fig. 1B) displayed a broad peak centered at about 2θ of 20°. The interlayer spacing in graphite (0.33 nm) was investigated, so these CQDs showed a graphitic nature with highly disordered carbon atoms (30).

The elementary composition of prepared CQDs was confirmed by elemental analysis to determine carbon, hydrogen, and nitrogen contents. The results were: C 37.26 wt.%, N 2.25 wt.%, H 4.07 wt.%, S 0.97 wt.%, and O (calculated) 55.45 wt.%. TEM images (Fig. 2) obviously showed that the CQDs were spherical, monodisperse, and had a narrow size distribution with the average diameters of about 16.3 ± 2.7 nm, with a maximum population at 8.5 nm.

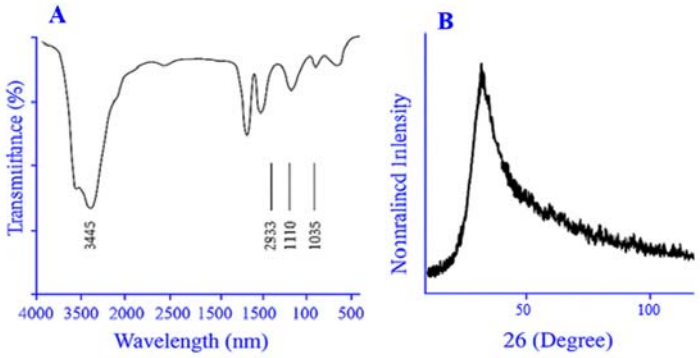

Fig. 1. (A) FTIR spectra and (B) XRD pattern of carbon quantum dots prepared from garlic juice.

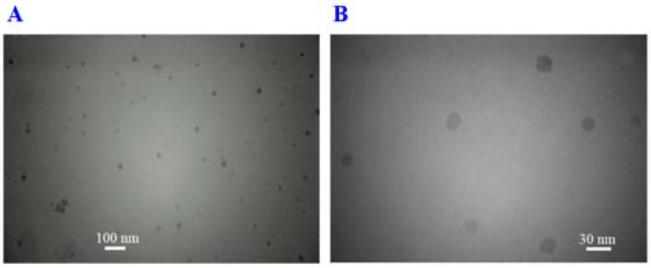

Fig. 2. TEM images at different magnifications of (A) 100 nm and (B) 30 nm of carbon quantum dots.

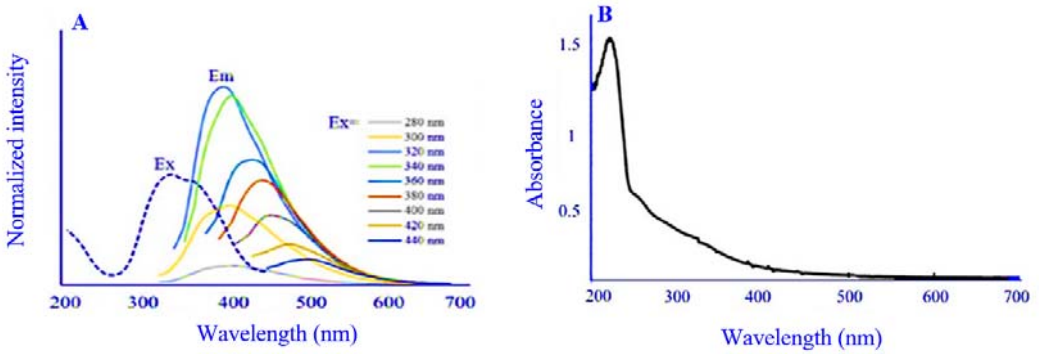

Fig. 3. (A) Excitation ($\lambda_{Emission}$ = 460 nm) and photoluminescence (at different excitation wavelengths) of carbon quantum dots, and (B) Absorption spectrum.

Optical properties of the CQDs

To further explore, the optical properties of the CQDs were investigated, as well as the photoluminescence and excitation spectra of the prepared CQDs at room temperature. The graphical representation of photoluminescence at various excitation wavelengths between 280 and 440 nm is illustrated in Fig. 3A. It demonstrates a typical excitation-dependent property. The maximum photoluminescence was exhibited at an excitation of 320 nm, with a maximum at 400 nm. The quantum efficiency of CQDs in a water-based solution was determined to be 11.5 at 340 nm excitation, employing quinine sulfate as the standard reference.

The UV-Vis absorption spectrum of CQDs, as illustrated in Fig. 3B, displays a distinct peak at 220 nm and a broader peak centered around 300 nm. According to the previous studies, these peaks can be attributed to π–π* and n-π* transitions of C=C and C=O bonds (31).

The effect of CQDs on cell viability and cellular fluorescence uptake

The potential of CQDs to trigger apoptosis in three types of human carcinoma cells (H1299, A549, and SKNMC) as well as normal cells (HUVEC) was evaluated using the MTT assay. CQDs were proven to be an outstandingly potent cytostatic agent, especially against H1299 cells, as confirmed by their IC_{50} value. As shown in Fig. 4A, exposure to CQDs for 48 h resulted in a concentration-dependent decrease in cell viability, with approximate IC_{50}s of 40 ± 2.39, 44.09 ± 4.1, and 19.3 ± 3.97 µg/mL in SKNMC, A549, and H1299 cells, respectively.

Therefore, in the next experiments, H1299 was selected for the identification of the mechanisms of CQD action. Figure 4B illustrates the effects of various CQD concentrations on the morphology of H1299 cells as opposed to untreated cells as the control. Exposure to CQDs resulted in observed phenomena like growth retardation, cellular shrinkage, vacuole formation, and mild cytoplasmic aggregations. Furthermore, a significant portion of the treated cells exhibited a spherical morphology and began to detach from the surface of the culture vessels. Also, as shown in Fig. 5, the intracellular fluorescence of CQDs increased concentration-dependently after exposure to different concentrations of CQDs in H1299 cells.

Effects of CQDs on caspase-3 and -9 activities

To finalize our findings and to characterize the nature of cell death observed in our experiments, the activity of caspase-3 and -9 in H1299 cells was investigated. The data obtained indicated a significant increase in caspase-3 activation in H1299 cells treated with CQDs at 20 and 40 µg/mL (Fig. 6A). To determine which apoptotic pathway is activated by CQDs, the activation of caspase-9, the apical proteases in the extrinsic pathway, was examined (32).

As shown in Fig. 6B, treatment with CQDs at 20 and 40 µg/mL significantly increased the activation of caspase-9 to 1.24 and 1.97-fold, compared to the control cells.

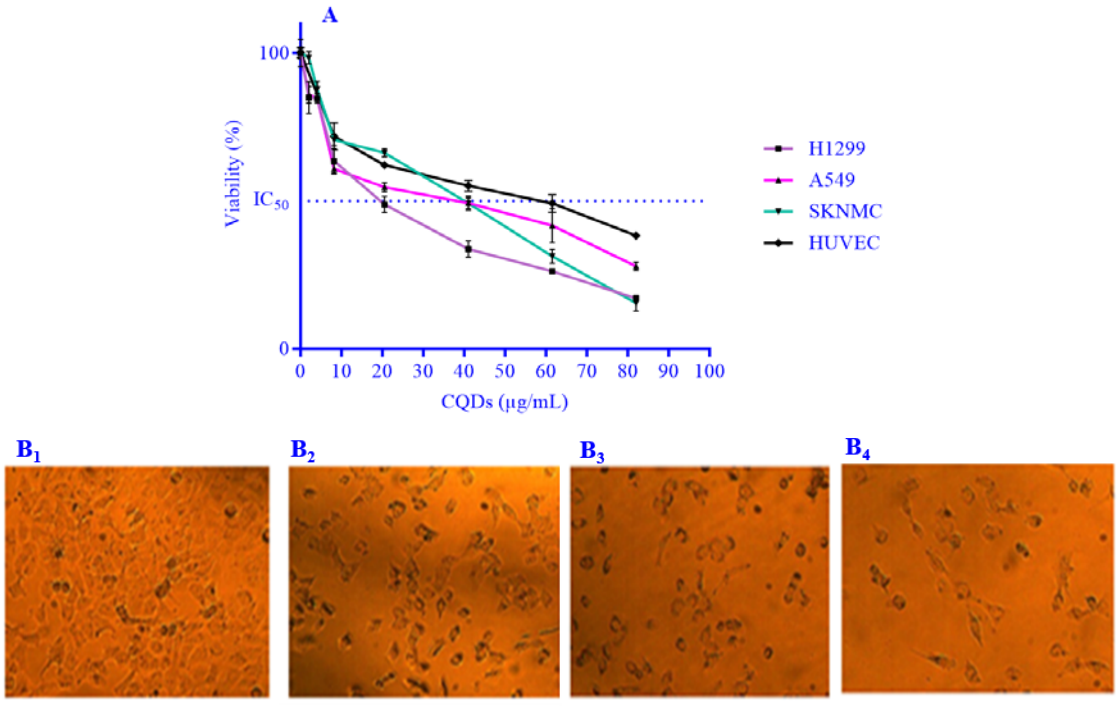

Fig. 4. Cytotoxic effects of CQDs in human carcinoma cell lines. (A) SKNMC, A549, H1299, and HUVEC cells were incubated with different concentrations of CQDs for 48 h. Data are presented as mean ± SEM (n = 3). (B) Representative photomicrograph shows morphological changes of H1299 cells; (B_1) untreated cells served as control, (B_2-B_4) cells treated with CQDs at 8, 20, and 40 µg/mL, respectively, for 48 h. CQD, carbon quantum dot.

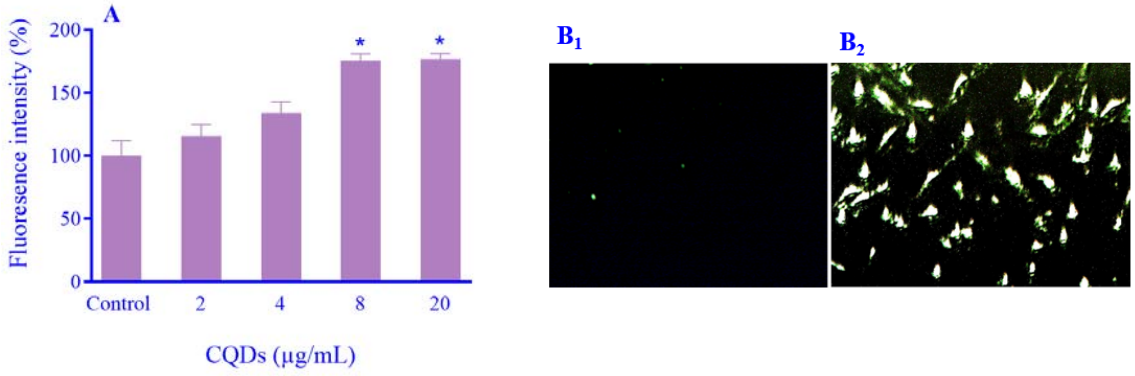

Fig. 5. (A) CQDs accumulation in H1299 cells after 2-h exposure to different concentrations of CQDs. Data are presented as mean ± SEM (n = 3). (B) Fluorescence microscope images demonstrating the intracellular CQDs distribution in human breast cancer cells; (B_1) untreated cells served as control, and (B_2) the cells exposed to CQDs at 20 µg/mL for 6 h. *$P < 0.05$ indicates significant differences in comparison with the control group. CQD, carbon quantum dot.

Effects of CQDs on MMP

We detected the effect of CQDs on the MMP in the H1299 cells. As shown in Fig. 7, when cells were treated with CQDs for 48 h at 37 °C, a considerable decrease in the retention of rhodamine 123 was observed at 20 and 40 µg/mL. Therefore, the disruption of the MMP triggered by CQDs led to damage in the outer membrane, causing the release of dye from the mitochondria and subsequently reducing intracellular fluorescence.

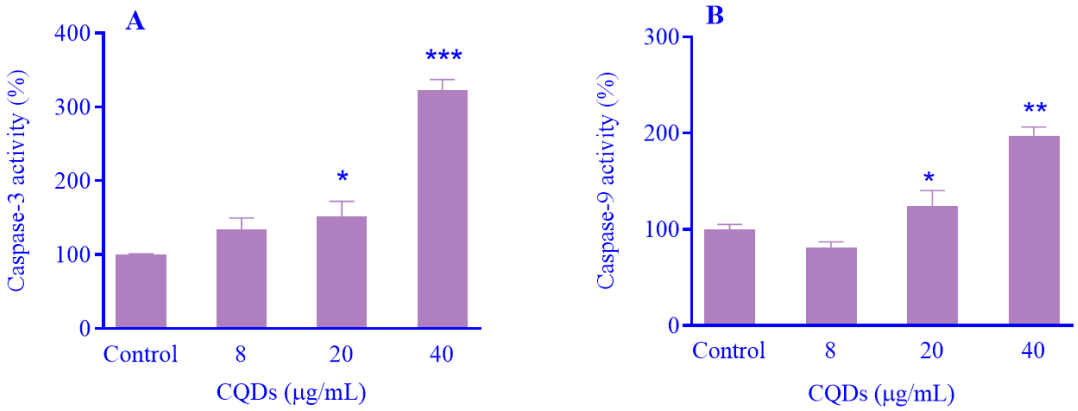

Fig. 6. The activity of (A) caspase 3 and (B) caspase 9 in H1299 carcinoma cells following treatment with various concentrations of CQDs for 24 h. Data are presented as the mean ± SEM, n = 3. *$P < 0.05$, **$P < 0.01$, and ***$P < 0.001$ indicate significant differences in comparison with the control group. CQD, carbon quantum dot.

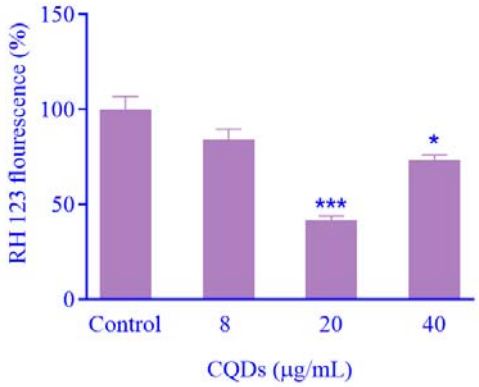

Fig. 7. CQDs-induced MMP collapse. Cells were treated with different concentrations of CQDs for 48 h. Graphs show the change in MMP as represented by the mean fluorescence intensity of rhodamine 123. Data are presented as the mean ± SEM, n = 3. *$P < 0.05$ and ***$P < 0.001$ indicate significant differences in comparison with the control group. CQD, carbon quantum dot; MMP, mitochondrial membrane potential.

DISCUSSION

In the current study, a simple, green, and large-scale synthesis of CQDs was done using hydrothermal treatment from a readily available natural precursor. These CQDs indicated a strong and stable photoluminescence effect that was dependent on excitation wavelength and pH. The fluorescence intensity of nitrogen-doped Carbon Quantum Dots (N-CDs) remained notably stable across a wide pH spectrum and upon exposure to UV radiation. The assessment was carried out on the cytotoxic effects of CQDs on three human carcinoma cell lines: H1299, A549, and SKNMC cells, alongside HUVEC as a normal cell line. The H1299 cell line was found to be the most sensitive to CQD (50% viability at 20 µg/mL), while CQD showed IC50 = 40 µg/mL against the SKNMC and A549 cell lines. In addition, HUVEC cells exhibited viability exceeding 50% when exposed to CQDs at concentrations of 20 and 40 µg/mL. However, when treated with CQDs at a concentration of approximately 50 µg/mL, the viability of HUVEC cells reached the 50% threshold.

The mechanism of inducing apoptosis, rather than necrosis, has been acknowledged as the primary mode of action for antitumor drugs (33). Consequently, substantial research endeavors are currently focused on the advancement of potential pharmaceuticals that trigger apoptosis in cancerous cells. In this particular investigation, the apoptotic

capabilities of CQD on the most responsive cell lines were scrutinized utilizing well-defined apoptosis markers. Caspases, a group of cysteine-dependent, aspartate-directed proteases, play a crucial part in the initiation and execution of apoptosis. Among these, caspase-3 is notably recognized as one of the predominantly involved caspases in prompting apoptosis in various cell types (7). Our analysis revealed that treatment with CQDs was associated with an increase in caspase-3 activity. Throughout apoptosis, there was a loss of MMP, leading to bioenergetic failure in mitochondria, thereby enabling the discharge of soluble molecules from the mitochondrial outer space into the cytosol (34). To assess the involvement of mitochondria in CQDs-induced apoptosis, the capacity of CQDs to alter MMP was examined, revealing a significant MMP decrease in the H1299 cell line after 48 h. In the course of mitochondria-dependent (intrinsic) apoptosis, alterations in the permeability of the mitochondrial outer membrane trigger the liberation of cytochrome c from the intermembrane space to the cytosol. This cytochrome c then united with apoptotic protease-activating factor-1 (Apaf-1) and d-ATP, forming a caspase-9-activating complex known as the apoptosome, which subsequently processed the procaspase-3 (35). Hence, we assessed the significance of the mitochondrial pathway in CQDs-mediated apoptosis by evaluating caspase-9 activity. Our findings distinctly indicated the crucial role of caspase-9 in CQDs-mediated apoptosis, as its activity surged after exposure to CQDs in H1299 cells. These outcomes suggest that the mitochondrial pathway holds a pivotal position in CQD-induced apoptosis. Hoong *et al.* have previously scrutinized the cytotoxic and apoptogenic effects of garlic extract on H1299 cells (36). Their study revealed a slight inhibition of cell growth by garlic extract (IC_{50} > 20 µ/mL) and illustrated the ability of garlic extract to trigger apoptosis in H1299 cells through an extrinsic pathway.

Additionally, earlier reports have demonstrated that crude garlic extract induced cell cycle arrest and heightened caspase activity (apoptosis) in the PC-3 human prostate cancer cell line (12).

CONCLUSION

In conclusion, our study demonstrated that CQDs have the capacity to induce apoptosis in non-small cell lung cancer cells. It was noted previously that expression was absent in H1299 cells, while the activation of apoptosis was facilitated by the involvement of the p53 tumor suppressor proteins in response to various internal and external stresses (4). Hence, the findings put forth imply that the process of apoptosis triggered by CQDs is governed through a pathway independent of p53.

Acknowledgments

The authors gratefully acknowledge the financial support provided by the Research Council of Kermanshah University of Medical Sciences (Grant No. 92283). This work was performed in partial fulfillment of the requirement for Pharm. D. thesis of E. Yosefi, in the Faculty of Pharmacy, Kermanshah University of Medical Sciences, Kermanshah, Iran.

Conflicts of interest statement

The authors declared no conflict of interest in this study.

Authors' contributions

F. Jalilian and A. Barati prepared the manuscript, analyzed the data, and performed statistical calculations; E. Yousefi conducted experimental studies and searched for previous studies; L. Hosseinzadeh and E. Arkan supervised the work, designed the study, corrected the manuscript, and provided the facilities for the study. All authors read and approved the finalized article.

REFERENCES

1. Sharma P, Brown S, Walter G, Santra S, Moudgil B. Nanoparticles for bioimaging. Adv Colloid Interface Sci. 2006;123:471-485. DOI: 10.1016/j.cis.2006.05.026.
2. Hutter E, Maysinger D. Gold nanoparticles and quantum dots for bioimaging. Microsc Res Tech. 2011;74(7):592-604. DOI:10.1002/jemt.20928.
3. Bungu L, van de Venter M, Frost C. Evidence for an *in vitro* anticoagulant and antithrombotic activity in *Tulbaghia violacea*. Afr J Biotechnol. 2008;7(6): 681-688.

4. Amaral JD, Xavier JM, Steer CJ, Rodrigues CM. The role of p53 in apoptosis. Discov Med. 2010;9(45):145-152. PMID: 20193641.
5. Smith AM, Duan H, Mohs AM, Nie S. Bioconjugated quantum dots for *in vivo* molecular and cellular imaging. Adv Drug Deliv Rev. 2008;60(11):1226-1240. DOI: 10.1016/j.addr.2008.03.015.
6. Apitz-Castro R, Cabrera S, Cruz MR, Ledezma E, Jain MK. Effects of garlic extract and of three pure components isolated from it on human platelet aggregation, arachidonate metabolism, release reaction and platelet ultrastructure. Thromb Res. 1983;32(2):155-169. DOI: 10.1016/0049-3848(83)90027-0.
7. Abbassi A. Yaghmaei P. Hosseinzadeh L. Cinnamaldehyde potentiates cytotoxic and apoptogenic effects of doxorubicin in prostate cancer cell line. Res Pharm Sci. 2024;19(4): 425-435. DOI: 10.4103/RPS.RPS_82_23.
8. Lewinski N, Colvin V, Drezek R. Cytotoxicity of nanoparticles. small. 2008;4(1):26-49. DOI: 10.1002/smll.200700595.
9. Xu X, Ray R, Gu Y, Ploehn HJ, Gearheart L, Raker K, *et al*. Electrophoretic analysis and purification of fluorescent single-walled carbon nanotube fragments. J Am Chem Soc. 2004;126(40):12736-12737. DOI: 10.1021/ja040082h.
10. Giard DJ, Aaronson SA, Todaro GJ, Arnstein P, Kersey JH, Dosik H, *et al*. *In vitro* cultivation of human tumors: establishment of cell lines derived from a series of solid tumors. J Natl Cancer Inst. 1973;51(5):1417-1423. DOI: 10.1093/jnci/51.5.1417.
11. Baker SN, Baker GA. Luminescent carbon nanodots: emergent nanolights. Angew Chem Int Ed Engl. 2010;49(38):6726-6744. DOI: 10.1002/anie.200906623.
12. Bagul M, Kakumanu S, Wilson TA. Crude garlic extract inhibits cell proliferation and induces cell cycle arrest and apoptosis of cancer cells *in vitro*. J Med Food. 2015;18(7):731-737. DOI: 10.1089/jmf.2014.0064.
13. Zhao S, Lan M, Zhu X, Xue H, Ng TW, Meng X, *et al*. Green synthesis of bifunctional fluorescent carbon dots from garlic for cellular imaging and free radical scavenging. ACS Appl Mater Interfaces. 2015;7(31):17054-17060. DOI: 10.1021/acsami.5b03228.
14. Yang C, Ogaki R, Hansen L, Kjems J, Teo BM. Theranostic carbon dots derived from garlic with efficient anti-oxidative effects towards macrophages. RSC Adv. 2015;5(118):97836-97840. DOI: 10.1039/C5RA16874K.
15. Hu SL, Niu KY, Sun J, Yang J, Zhao NQ, Du XW. One-step synthesis of fluorescent carbon nanoparticles by laser irradiation. J Mater Chem. 2009;19(4):484-488. DOI: 10.1039/B812943F.
16. Bhunia SK, Saha A, Maity AR, Ray SC, Jana NR. Carbon nanoparticle-based fluorescent bioimaging probes. Sci Rep. 2013;3:1473,1-7. DOI: 10.1038/srep01473.
17. Briscoe J, Marinovic A, Sevilla M, Dunn S, Titirici M. Biomass-derived carbon quantum dot sensitizers for solid-state nanostructured solar cells. Angew Chem Int Ed Engl. 2015;54(15):4463-4468. DOI: 10.1002/anie.201409290.
18. Qu S, Wang X, Lu Q, Liu X, Wang L. A biocompatible fluorescent ink based on water-soluble luminescent carbon nanodots. Angew Chem Int Ed Engl. 2012;51(49):12215-12218. DOI: 10.1002/anie.201206791.
19. Arkan E, Barati A, Rahmanpanah M, Hosseinzadeh L, Moradi S, Hajialyani M. Green synthesis of carbon dots derived from walnut oil and an investigation of their cytotoxic and apoptogenic activities toward cancer cells. Adv Pharm Bull. 2018;8(1):149-155. DOI: 10.15171%2Fapb.2018.018.
20. Barati A, Shamsipur M, Arkan E, Hosseinzadeh L, Abdollahi H. Synthesis of biocompatible and highly photoluminescent nitrogen doped carbon dots from lime: analytical applications and optimization using response surface methodology. Mater Sci Eng C Mater Biol Appl. 2015;47:325-332. DOI: 10.1016/j.msec.2014.11.035.
21. Prasannan A, Imae T. One-pot synthesis of fluorescent carbon dots from orange waste peels. Ind Eng Chem Res. 2013;52(44):15673-15678. DOI: 10.1021/ie402421s.
22. Mehta VN, Jha S, Basu H, Singhal RK, Kailasa SK. One-step hydrothermal approach to fabricate carbon dots from apple juice for imaging of mycobacterium and fungal cells. Sens Actuators B Chem. 2015;213:434-443. DOI: 10.1016/j.snb.2015.02.104.
23. Hsu PC, Chen PC, Ou CM, Chang HY, Chang HT. Extremely high inhibition activity of photoluminescent carbon nanodots toward cancer cells. J Mater Chem B. 2013;1(13):1774-1781. DOI: 10.1039/C3TB00545C.
24. Nouroz F, Mehboob M, Noreen S, Zaidi F, Mobin T. A review on anticancer activities of garlic (*Allium sativum L.*). Middle East J Sci Res. 2015;23(6):1145-1151. DOI: 10.5829/idosi.mejsr.2015.23.06.9381.
25. Sun C, Zhang Y, Wang P, Yang Y, Wang Y, Xu J, *et al*. Synthesis of nitrogen and sulfur co-doped carbon dots from garlic for selective detection of Fe 3+. Nanoscale Res Lett. 2016;11:1-9. DOI: 10.1186/s11671-016-1326-8.
26. Miroddi M, Calapai F, Calapai G. Potential beneficial effects of garlic in oncohematology. Mini-Rev Med Chem. 2011;11(6):461-472. DOI: 10.2174/138955711795843293.
27. Sun X, Li Y. Colloidal carbon spheres and their core/shell structures with noble-metal nanoparticles. Angew Chem Int Ed Engl. 2004;43(5):597-601. DOI: 10.1002/ange.200352386.
28. Shokoohinia Y, Hosseinzadeh L, Alipour M, Mostafaie A, Mohammadi-Motlagh HR. Comparative evaluation of cytotoxic and apoptogenic effects of several coumarins on

human cancer cell lines: osthole induces apoptosis in p53-deficient H1299 cells. Adv Pharmacol Pharm Sci. 2014;2014:1-8.
DOI: 10.1155/2014/847574.
29. Perry SW, Norman JP, Barbieri J, Brown EB, Gelbard HA. Mitochondrial membrane potential probes and the proton gradient:a practical usage guide. Biotechniques. 2011;50(2):98-115.
DOI: 10.2144/000113610.
30. Li H, Kang Z, Liu Y, Lee ST. Carbon nanodots: synthesis, properties and applications. J Mater Chem. 2012;22(46):24230-24253.
DOI: 10.1039/C2JM34690G.
31. Yu P, Wen X, Toh YR, Tang J. Temperature-dependent fluorescence in carbon dots. J Phys Chem C. 2012;116(48):25552-25557.
DOI: 10.1021/jp307308z.
32. Hosseinzadeh L, Behravan J, Mosaffa F, Bahrami G, Bahrami A, Karimi G. Curcumin potentiates doxorubicin-induced apoptosis in H9c2 cardiac muscle cells through generation of reactive oxygen species. Food Chem Toxicol. 2011;49(5):1102-1109.
DOI: 10.1016/j.fct.2011.01.021.
33. Jalilian F, Moieni-Arya M, Hosseinzadeh L, Shokoohinia Y. Oxypeucedanin and isoimperatorin extracted from *Prangos ferulacea (L.)* Lindl protect PC12 pheochromocytoma cells from oxidative stress and apoptosis induced by doxorubicin. Res Pharm Sci. 2022;17(1):12-21.
DOI: 10.4103/1735-5362.329922.
34. Abbasi A, Hajialyani M, Hosseinzadeh L, Jalilian F, Yaghmaei P, Jamshidi Navid S, *et al*. Evaluation of the cytotoxic and apoptogenic effects of cinnamaldehyde on U87MG cells alone and in combination with doxorubicin. Res Pharm Sci. 2020; 15(1):26-35.
DOI: 10.4103/1735-5362.278712.
35. Shokoohinia Y, Hosseinzadeh L, Moieni-Arya M, Mostafaie A, Mohammadi-Motlagh HR. Osthole attenuates doxorubicin-induced apoptosis in PC12 cells through inhibition of mitochondrial dysfunction and ROS production. Biomed Res Int. 2014;2014: 1-7.
DOI: 10.1155/2014/156848.
36. Hong YS, Ham YA, Choi JH, Kim J. Effects of allyl sulfur compounds and garlic extract on the expressions of Bcl-2, Bax, and p53 in non small cell lung cancer cell lines. Exp Mol Med. 2000;32(3): 127-134.
DOI: 10.1038/emm.2000.22.